

See discussions, stats, and author profiles for this publication at: <http://www.researchgate.net/publication/276656402>

Effect of anisotropies on the magnetization dynamics

ARTICLE *in* NETWORKS AND HETEROGENEOUS MEDIA · MARCH 2015

Impact Factor: 0.65 · DOI: 10.3934/nhm.2015.10.209

READS

20

7 AUTHORS, INCLUDING:



O.J. Suarez

University of Tarapacá

10 PUBLICATIONS 84 CITATIONS

[SEE PROFILE](#)



Jason A C Gallas

Universidade Federal da Paraíba

169 PUBLICATIONS 2,534 CITATIONS

[SEE PROFILE](#)



Hector L. Mancini

Universidad de Navarra

94 PUBLICATIONS 1,618 CITATIONS

[SEE PROFILE](#)



J. Bragard

Universidad de Navarra

53 PUBLICATIONS 592 CITATIONS

[SEE PROFILE](#)

EFFECT OF ANISOTROPIES ON THE MAGNETIZATION DYNAMICS

LAURA M. PÉREZ, JEAN BRAGARD AND HECTOR MANCINI

Departamento de Física y Matemáticas Aplicadas
Universidad de Navarra, Pamplona, 31080, Spain

JASON A. C. GALLAS

Departamento de Física
Universidade Federal da Paraíba, 58051-970 João Pessoa, Brazil
and
Institute for Multiscale Simulation
Friedrich-Alexander-Universität Erlangen-Nürnberg
Nägelsbachstraße 49b, 91052 Erlangen, Germany

ANA M. CABANAS

Instituto de Alta Investigación
Universidad de Tarapacá, Casilla 7D, Arica, Chile

OMAR J. SUAREZ

Instituto de Alta Investigación
Universidad de Tarapacá, Casilla 7D, Arica, Chile
and
Departamento de Matemáticas y Física
Universidad de Sucre, A.A. 406, Sincelejo, Colombia

DAVID LAROZE

Instituto de Alta Investigación
Universidad de Tarapacá, Casilla 7D, Arica, Chile
and
SUPA School of Physics and Astronomy
University of Glasgow, Glasgow G12 8QQ, United Kingdom

ABSTRACT. We report a systematic investigation of the magnetic anisotropy effects observed in the deterministic spin dynamics of a magnetic particle in the presence of a time-dependent magnetic field. The system is modeled by the Landau-Lifshitz-Gilbert equation and the magnetic field consists of two terms, a constant term and a term involving a harmonic time modulation. We consider a general quadratic anisotropic energy with three different preferential axes. The dynamical behavior of the system is represented in Lyapunov phase diagrams, and by calculating bifurcation diagrams, Poincaré sections and Fourier spectra. We find an intricate distribution of shrimp-shaped regular island embedded in wide chaotic phases. Anisotropy effects are found to play a key role in defining the symmetries of regular and chaotic stability phases.

2010 *Mathematics Subject Classification.* Primary: 37M25, 65P20; Secondary: 65P99.

Key words and phrases. Spin dynamics, anisotropy, chaos, Lyapunov exponents, Fourier analysis.

1. Introduction. The understanding of the dynamical processes involved in the magnetization of generic nanoparticles is a quite interesting and challenging problem. Indeed, this problem contains several complex phenomena which include multistability, quasiperiodicity, deterministic chaos, as well as complicated pattern formation and evolution [54, 41, 32]. Experimentally, the detection and classification of such complex behaviors is a virtually impossible task because it presupposes the ability of tuning material properties continuously over rather extended parameter ranges and external conditions. Theoretically, the description of stability phases has been frequently restricted to the study of fixed-points, Hopf bifurcations and other simple informations which are routinely derived from the equations of motion.

However, the availability of fast computer clusters combined with realistic models offer the possibility to simulate more complicated dynamical processes numerically like, e.g. periodic solutions with arbitrary period length and waveforms, and to discover novel material properties of interest. In this context, a first problem that needs to be tackled is the determination of the control parameter regions that support chaotic and regular behaviors. More specifically, one needs to compute phase diagrams displaying chaotic and regular stable phases, their extension and the detailed shape of their boundaries. When dealing with nonlinear dynamical systems, phase diagrams are frequently restricted to just a few isolated curves displaying boundaries between steady-state (fixed-points) solutions and solutions emerging immediately after them, either by Hopf or by other simple bifurcations. Furthermore, existing phase diagrams tend to focus on unstable mathematical phenomena and/or situations that are not accessible in the laboratory. Even though deterministic chaos has been studied intensively for over 30 years, phase diagrams detailing the structure of chaotic phases with high-resolution have started to be reported only quite recently. For recent surveys on this subject see, for example, Refs. [45, 29].

Nonlinear problems have been widely studied in magnetism [54, 41, 32]. Models were used both for discrete [3, 52, 34, 35, 36, 46, 15, 37, 38, 44] and for continuous magnetic systems [41, 32, 4, 17, 18, 50, 51]. Recently, the chaotic behavior of an uni-axial anisotropic particle under a periodic magnetic field was studied in Refs.[15, 37]. Several experiments of chaotic behaviors in magnetic systems have been reported [30, 1, 8, 16]. Typical magnetic samples are yttrium iron garnet spheres [30]. It is worth mentioning that ferromagnetic resonance techniques have allowed to uncover different routes to chaos, such as period-doubling cascades, quasi-periodic routes to chaos, or intermittent routes. This obviously implies that there is no universal mechanism leading to chaos in these systems and, therefore, that a theoretical description turns out to be highly non-trivial.

The characterization of the chaotic and regular phases using two-dimensional phase diagrams displaying the largest Lyapunov of the exponents for a parametrically driven uni-axial anisotropic magnetic particle has been recently studied in Refs.[15, 37]. Since this type of anisotropy is a special one [41, 19], the aim of the present manuscript is to investigate a more general system where one combines different anisotropy axes. This new assumption on the structure of the anisotropy will modify the dynamical behaviors of the particles. The main goal of the present study is to illustrate this more general setup. To this end, we have solve numerically the dimensionless Landau-Lifshitz-Gilbert (LLG) equation containing a general quadratic anisotropic energy. The paper is organized as follows: In Section 2, the

theoretical model for a magnetic particle with a general quadratic anisotropy energy is presented. In Section 3 we report the numerical simulations together with a discussion of the results. Finally, our conclusions are presented in Section 4.

2. Theoretical model. Let us consider a magnetic particle and assume that it can be represented by a magnetic monodomain of magnetization \mathbf{M} governed by the dimensionless LLG equation

$$\kappa \frac{d\mathbf{m}}{d\tau} = -\mathbf{m} \times \boldsymbol{\Gamma} - \eta \mathbf{m} \times (\mathbf{m} \times \boldsymbol{\Gamma}), \quad (1)$$

where $\mathbf{m} = \mathbf{M}/M_s$, $\tau = t|\gamma|M_s$ and $\kappa = 1 + \eta^2$ [41, 3]. Here M_s is the saturation magnetization that leads to $|\mathbf{m}| = 1$, and γ is the gyromagnetic factor, which is associated with the electron spin and whose numerical value is approximately given by $|\gamma| = |\gamma_e|\mu_0 \approx 2.21 \times 10^5 \text{ mA}^{-1}\text{s}^{-1}$. Here, η denotes the dimensionless phenomenological damping coefficient, a material property typically in the range from 10^{-4} to 10^{-3} in garnets and 10^{-2} , or larger in cobalt or in nickel or in permalloy [37], giving $1/\kappa \approx 0.99 \simeq 1$. Typical experimental values of M_s are, e.g. $M_{s[\text{Co}]} \approx 1.42 \times 10^6 \text{ A/m} \approx 17.8 \text{ kOe}$ for cobalt materials and $M_{s[\text{Ni}]} \approx 4.8 \times 10^5 \text{ A/m} \approx 6 \text{ kOe}$ for nickel materials, leading to $|\gamma|M_{s[\text{Co}]} \approx 308 \text{ GHz}$ and $|\gamma|M_{s[\text{Ni}]} \approx 106 \text{ GHz}$, respectively. Hence, the corresponding time scales are $(|\gamma|M_s)^{-1} \approx 3 \text{ ps}$ and $(|\gamma|M_s)^{-1} \approx 6 \text{ ps}$, respectively. Let us remark that in these materials the macrospin approximation (monodomain particles) is valid for particles sizes in the range of $10 - 20 \text{ nm}$, because for smaller sizes surface anisotropy effects (not included in the present study) are relevant [7] and for larger sizes non-uniform magnetic states appear, like vortices in cobalt nanodots. In addition, the shape of the particle plays an important role in the macrospin approximation [33]. Finally, the fact that $|\mathbf{m}|$ is conserved implies automatically that Eq. (1) describes pure rotations of the magnetization in 3D space.

The effective magnetic field, denoted by $\boldsymbol{\Gamma}$ in Eq.(1), is given by

$$\boldsymbol{\Gamma} = \mathbf{h} + \sum_{j=1}^3 \alpha_j (\mathbf{m} \cdot \hat{\mathbf{n}}_j) \hat{\mathbf{n}}_j, \quad (2)$$

where \mathbf{h} is the external magnetic field and α_j measures the anisotropy along the \mathbf{n}_j axis, such that subindexes (1, 2, 3) represent the principal axes. We denote them in Cartesian coordinates as (x, y, z) . We apply an external magnetic field \mathbf{h} that comprises both, a constant longitudinal and a periodic transverse part with fixed amplitude and frequency

$$\mathbf{h} = \mathbf{h}_0 + \mathbf{h}_T \sin(\Omega\tau), \quad (3)$$

where \mathbf{h}_0 ($\parallel \hat{\mathbf{z}}$), \mathbf{h}_T ($\perp \hat{\mathbf{z}}$) and Ω are time independent. With this dimensional scaling, the dimensionless fields and frequencies are $\mathbf{h} = \mathbf{H}/M_s$ and $\Omega = \omega/(\gamma M_s)$. Since the amplitude of field and the frequency are measured in units of M_s and (γM_s) , respectively, one finds that for cobalt or nickel materials the typical order of magnitude is $10^0 - 10^1 \text{ kOe}$ and GHz . Here, we vary these values in the same range of magnitude.

The second term of the right-hand-side of the Eq. (2) corresponds to the anisotropy field. This term comes from anisotropy energy which essentially takes into account the fact that the magnetic properties depend of the direction in which they are measured [19]. This energy has contributions from different natures, like crystal, magneto-static, or shape anisotropy.

To first-order of approximation, the characterization of the anisotropy effect is obtained by including the quadratic terms of \mathbf{m} in the magnetic energy. In the principal axes representation, these terms give our prototype field [41, 19]. Let us remark that there are two special cases. The first one, called *uniaxial anisotropy*, involves two coefficients which are zero. The standard configuration for this case is $\alpha_x = \alpha_y = 0$, and $\alpha_z \neq 0$. The second particular case, that we call *bi-axial anisotropy*, occurs when only a single coefficient is zero, for instance $\alpha_z = 0$. The coefficients α_j are related to the physical values through $\alpha_j = 2K_j/(\mu_0 M_s^2) - N_j$ where K_j are the physical anisotropy constants and N_j are the dimensionless demagnetizing factors which depend of the particle shape [33, 48, 49, 10]. The values of the anisotropy can be positive or negative, depending on the specific material and sample shape in use [19, 42].

From the dynamical point of view, it is worth mentioning that anisotropic particles under stationary magnetic field have been studied previously in some particular cases in Ref. [41] and uni-axial anisotropic particles under time-dependent magnetic field have been numerically characterized in Refs. [3, 46, 15, 37, 38].

Finally, let us remark that for zero damping ($\eta = 0$) and without parametric forcing ($h_x = h_y = 0$) Eq.(1) is conservative, and its dynamics can be derived from a free energy functional, giving stationary or periodic solutions. Therefore, the inclusion of the dissipation and the oscillatory injection of energy drives the precessional dynamics into multiple instabilities. In such circumstance the magnetization of the particle may exhibit complex dynamical behavior, e.g., quasi-periodicity, and chaos [3, 15, 37]. In the next Section we provide a more exhaustive characterization of the chaotic regime, including its dependence on the anisotropy constants as well as on the magnetic field amplitudes, which shows elaborate and entangled patterns.

3. Simulations. This Section is divided into two parts. In the first subsection we briefly discuss the quantities, which we use to characterize temporal regimes, and in the second one some numerical results and their analysis are provided.

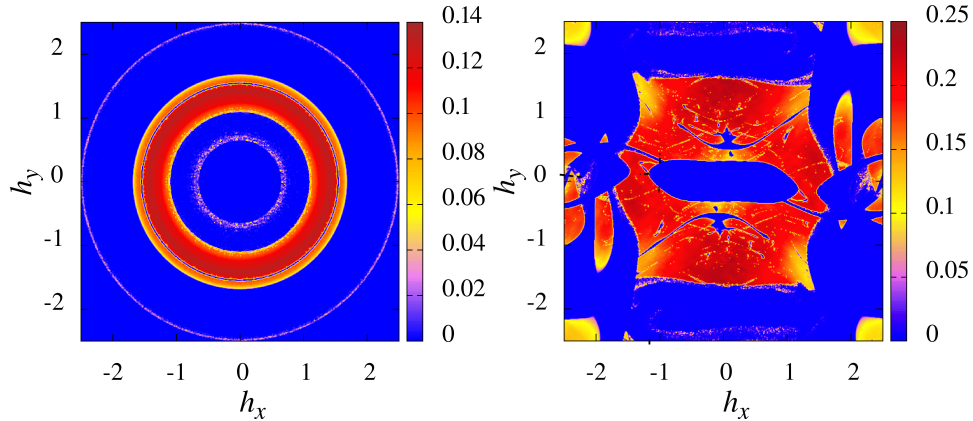


FIGURE 1. (Color online) Phase diagrams displaying the largest Lyapunov exponent (LLE) color-coded as a function of the amplitudes h_x and h_y for $\alpha_x = \alpha_y = 1.0$ (left) and $\alpha_x = -\alpha_y = 1.0$ (right). The fixed parameters are: $\Omega = 1.0$, $h_z = 0.1$, $\alpha_z = 0$ and $\eta = 0.05$. The resolutions are $\Delta h_x = \Delta h_y = 0.01$.

3.1. Dynamical indicators. First, we characterize the dynamics of Eq. (1) by evaluating the Lyapunov exponents (LEs). This method consists of quantifying the divergence between two initially close trajectories of a vector field [55, 28]. In general, for an effective N-dimensional dynamical system described by a set of equations, $dX^i/d\tau = F^i(\mathbf{X}, \tau)$, the ith-Lyapunov exponent is given by

$$\lambda_i = \lim_{\tau \rightarrow \infty} \left(\frac{1}{\tau} \ln \left(\frac{\|\delta X_\tau^i\|}{\|\delta X_0^i\|} \right) \right), \quad (4)$$

where $\|\delta X_\xi^i\|$ is the distance between the trajectories of the ith-component of the vector field at time ξ . They can be ordered from the largest to the smallest: $\lambda_1 \geq \lambda_2 \geq \dots \geq \lambda_N$. The first exponent is the largest Lyapunov exponent (LLE). Due to the fact that the LLG equation conserves the modulus of the magnetization $|\mathbf{m}|$ and that the applied magnetic field is time dependent, the effective dimension of the phase space is three. From a dynamical system point of view, only the largest LLE may become positive for a system of dimension three. Therefore, by exploring the dependence of the LLE on the different parameters of the system, one can identify areas in control parameter space, where the dynamics is chaotic (LLE positive), and those showing nonchaotic dynamics (LLE vanishing or negative). Nevertheless, let us comment that since we are dealing with a one-frequency forced system, at least one of its Lyapunov exponents is always zero; hence the simplest attractor is a periodic orbit. Another possibility is to have two or three Lyapunov exponents equal to zero and in these cases the system exhibits a two or three-frequency quasi-periodic behavior.

Apart from the Lyapunov spectrum analysis, there are other methods of quantifying the dynamical behavior of a system, for example, the Fourier spectrum, Poincaré sections, or correlation functions just to mention few of them [54, 41, 52, 34, 3, 46, 15, 20, 39]. The classical technique to understand the time series of each components of \mathbf{m} is to take the Fast Fourier Transform (FFT) which gives a complex discrete signal, $S(\varpi)$, in frequency space $\varpi = (\varpi_1, \dots, \varpi_n)$, producing a set of pairs $\{\varpi_k, S(\varpi_k)\}$. For this signal we calculate its power spectrum $|S(\varpi)|$. In general, when $|S(\varpi)|$ has a finite number of discrete peaks, the time series is regular, while if there is a *continuum* of peaks, the series can be chaotic. Let us mention that the bifurcation diagrams using Poincaré sections of the magnetization angles, given by $\mathbf{m} = (\cos \phi \sin \theta, \sin \phi \sin \theta, \cos \theta)$, was employed in Ref. [3] while the local maximum of a specific component of \mathbf{m} was used in Ref. [46]. In these diagrams, when there is a continuum of points in the variable the behavior is quasi-periodic or chaotic.

3.2. Numerical results. Many numerical schemes have been used to resolve the LLG equation [41] and to avoid numerical artifacts, it is convenient to solve Eq. (1) in the Cartesian coordinates [3]. In order to find the chaotic regimes, we have integrated Eq. (1) via a standard fourth-order Runge-Kutta integration scheme with a fixed time step $d\tau = 0.01$ guaranteeing a precision of 10^{-8} for the magnetization field. The Lyapunov exponents are calculated using the technique exposed in Refs. [15, 55], such that the LEs are calculated for a time span of $\tau = 32768$ units of time after an initial transient time of $\tau = 1024$ units has been discarded. The Gram-Schmidt orthogonalization process is performed after every $\delta\tau = 1$. The error Err in the evaluation of the LEs has been checked by using $Err = \sigma(\lambda_M) / \max(\lambda_M)$, where $\sigma(\lambda_M)$ is the standard deviation of the maximum positive LE. In all cases

studied here Err is of the order of 1% or less, which is sufficiently small for the purpose of the present analysis.

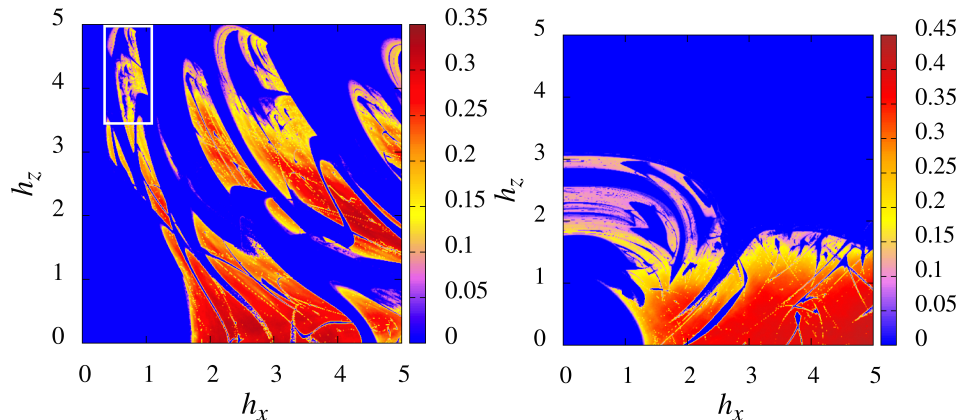


FIGURE 2. (Color online) Phase diagrams displaying the largest Lyapunov exponent (LLE) color-coded as a function of the amplitudes h_z and h_x for $(\alpha_x, \alpha_y, \alpha_z) = (4.0, 0, -1.0)$ (left) and $(\alpha_x, \alpha_y, \alpha_z) = (0, 4.0, 1.0)$ (right). The fixed parameters are: $\Omega = 1.0$, $h_y = 1.0$ and $\eta = 0.05$. The resolutions are $\Delta h_z = \Delta h_x = 0.01$.

The main results are given in Figs. 1–6. In particular, we discuss the influence of the magnetic field amplitudes and the anisotropy constants on the dynamics. The choice of parameters ensures realistic values and avoids possible artifacts due to a specific system and, therefore, provides a general description. Due to the large number of control parameters involved in the system, we fix $\Omega = 1$ and $\eta = 0.05$ for the rest of the manuscript.

We compute two-dimensional phase diagrams illustrating the magnitude of the LLE as a function of two parameters. This allows us to determine the parameter ranges that lead to chaotic dynamics, i.e. positive LLEs, and those showing regular (periodic or quasi-periodic) dynamics, LLEs zero or negative. In addition, following a technique explained in Ref. [28], we use an iterative zoom resolution process to investigate further the dependence of the dynamics upon very small variations of system parameters. This technique is generally used for studying dynamical systems that contain chaotic phases with highly complicated and interesting boundary topologies, e.g., curves where networks of stable islands of regular oscillations with ever-increasing periodicities accumulate systematically.

Figure 1 shows a color-coded LLE phase diagram as a function of the oscillatory field amplitudes h_x and h_y for a bi-axial anisotropic particle ($\alpha_z = 0$). The left panel displays the case when both anisotropy constants have the same value ($\alpha_x = \alpha_y = 1$). In this case, the chaotic regions appear in a circular symmetric fashion pointing out an invariance of the LEs with respect to the orientation of \mathbf{h}_T . Since the occurrence of chaos is independent of initial conditions and since there is only a single basin of attraction for the dynamics, the orientation of \mathbf{h}_T in the perpendicular plane is irrelevant for the position of the regions with positive LEs. We observe that no chaos is found for small amplitudes of the oscillatory

transverse field and that by increasing the field amplitudes, regions with chaos and regions with regular dynamics alternate. The right panel in Fig. 1 shows the case when anisotropy constants have opposite signs ($\alpha_x = -\alpha_y = 1$). We observe that the circular symmetry is broken and a pattern of chaotic-regular regions appears. Nevertheless, the LLE has a mirror-inversion symmetry with respect to $h_y = 0$ and $h_x \rightarrow -h_x$. We can also observe that for small values of both amplitudes, approximately inside the region, $0.761h_x^2 + 1.1h_xh_y + 8.232h_y^2 = 1$, the system presents regular states.

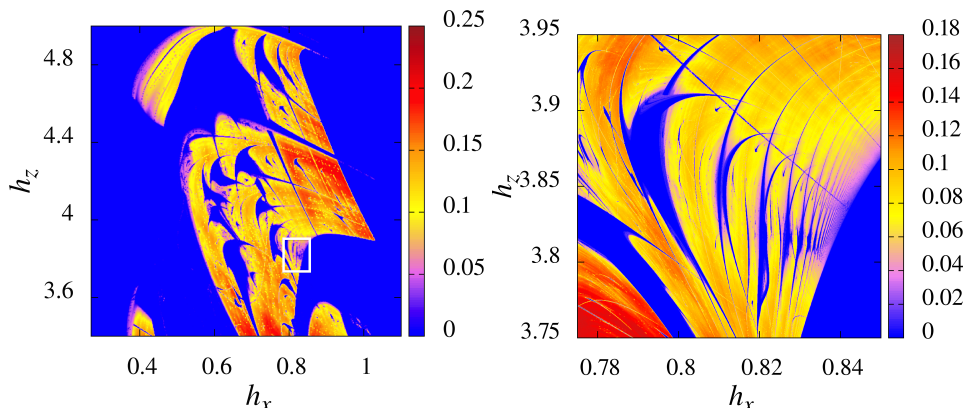


FIGURE 3. (Color online) (left) Magnification of the white box in the left panel of Figure 2. (right) Magnification of the white box in this left panel. The resolutions are $(\Delta h_z, \Delta h_x) = (0.0032, 0.00166)$ and $(\Delta h_z, \Delta h_x) = (2.0 \times 10^{-4}, 7.5 \times 10^{-5})$, respectively.

Figure 2 shows a color-coded LLE phase diagram given as a function of the field amplitudes h_x and h_z of the periodic transverse and constant longitudinal fields, respectively. We focus on two different cases of bi-axial anisotropic particle. In the left panel the principal axes are $(\hat{\mathbf{x}}, \hat{\mathbf{z}})$, while in the second panel they are $(\hat{\mathbf{y}}, \hat{\mathbf{z}})$. In the left panel we can observe that for the complete range of h_z studied, regular solutions are found for small values of h_x ($h_x \lesssim 0.3$). For intermediate and large values of h_z , one observes again an alternation of chaotic and regular regions as h_x increases. On the other hand, the right panel of Fig. 2 shows that chaos is suppressed for small values of both fields approximately inside the disk defined by $h_x^2 + h_z^2 = 1.2$. Chaotic behavior is not observed for intermediate and higher values of longitudinal field ($h_z \gtrsim 3$) irrespective of the value of h_x , indicating that the longitudinal field stabilizes the system. In the rest of the plotted area the chaotic regions are not compact, but contain many areas of regular dynamics for specific values of the field amplitudes.

In order to explore in more detail the transitions among chaotic and regular states, Figure 3 shows two successive magnifications of the left panel of Figure 2. These magnifications are performed with higher resolution. In the left phase diagram we can observe that there are special types of regular islands inside of chaotic region. In fact, these islands have the shape of *shrimps*, structures that were first discovered in the Hénon map [27] and, subsequently, have been found abundantly in multiple branches of physics [28, 40, 21, 53, 23, 26, 11, 12, 43, 6, 2, 22]. Finally, the magnification seen on the right panel of Figure 3 reveals an interesting pattern in the

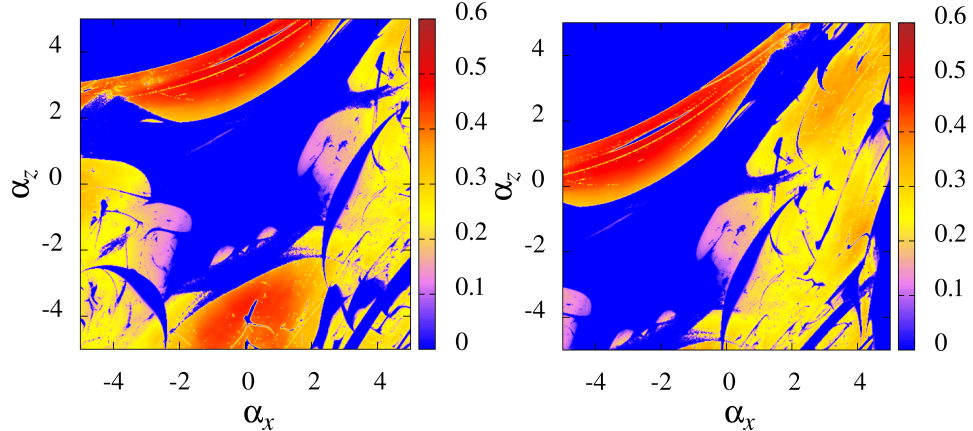


FIGURE 4. (Color online) Phase diagrams illustrating the largest Lyapunov exponent (LLE) color-coded as a function of the anisotropy constants α_z and α_x at $\alpha_y = 0$ (left) and $\alpha_y = -2.5$, (right). The fixed parameters are: $\Omega = 1.0$, $h_x = 2.45$, $h_y = 2.45$, $h_z = 0.1$, and $\eta = 0.05$. The resolutions in both cases are $\Delta\alpha_x = \Delta\alpha_z = 0.02$. Note that the parameter change seems to simply shift the panels, one with respect to the other.

form of a regular self-similar succession of shrimps with characteristic accumulation boundaries in phase diagrams [13].

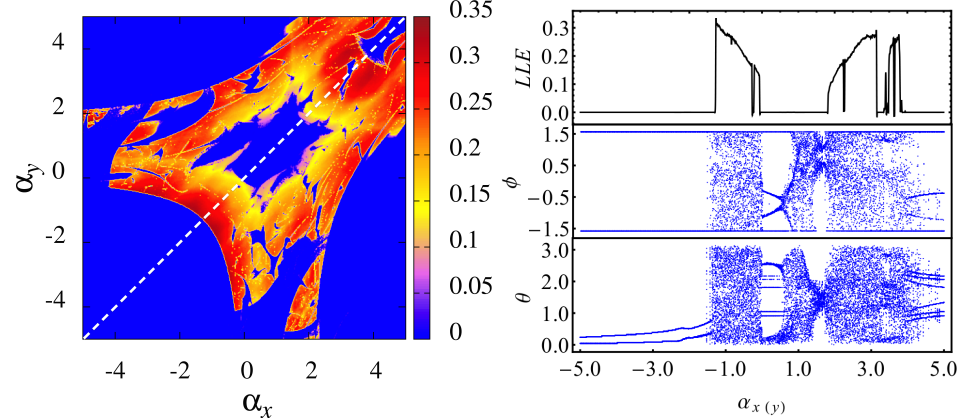


FIGURE 5. (Color online) (left) Phase diagram displaying the largest Lyapunov exponent (LLE) color-coded as a function of the anisotropy constants α_x and α_y . The fixed parameters are: $\Omega = 1.0$, $h_x = 1.0$, $h_y = 1.0$, $h_z = 0.1$, $\alpha_z = 1.0$ and $\eta = 0.05$. The resolutions are $\Delta\alpha_z = \Delta\alpha_x = 0.02$. (right) LLE and bifurcation diagrams of ϕ and θ as a function of the diagonal (white-) line $\alpha_{y(x)}$ given in the left panel.

Next, let us characterize the influence of the anisotropy constants on the resulting dynamical behavior. Figure 4 shows phase diagrams as a function of the anisotropy

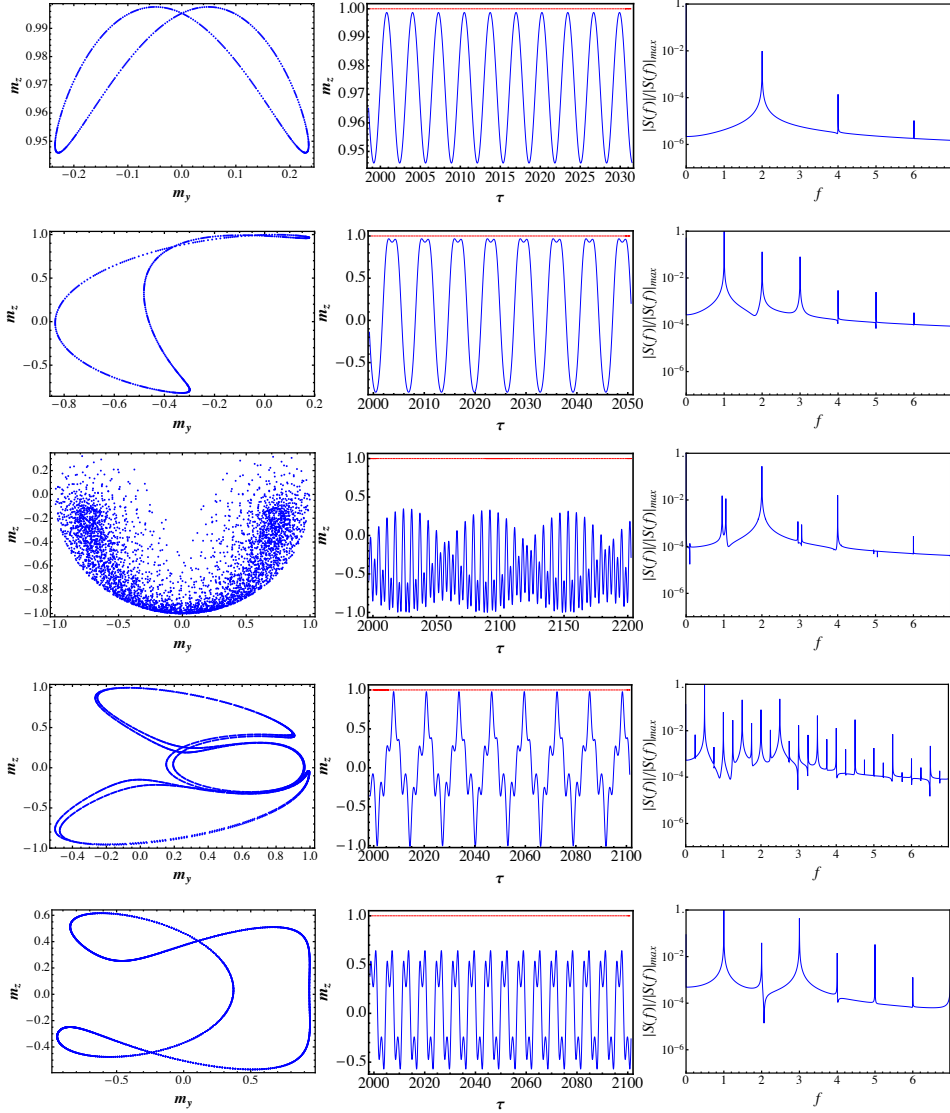


FIGURE 6. 2D Poincaré sections of (m_z, m_y) taken at time interval multiples of $2\pi/\Omega$, the time series of m_z , and its corresponding power spectrum $|S(\varpi)|$ for $\alpha_{y(x)} = (-3.5, -0.3, 0.95, 3.27, 4.95)$. The dashed line in the time series represents $|\mathbf{m}|$. The other fixed parameters are the same as the ones used in Figure 5.

coefficients α_x and α_z for $\alpha_y = 0$ (left) and $\alpha_y = -2.5$ (right). The case $\alpha_y = 0$ is again for a bi-axial particle, nonetheless the LLE diagram exposes a quite complex scenario without any symmetry. In the parameter region where the anisotropies are small and intermediate ($-1.7 \lesssim \alpha_x \lesssim 1.5$ and $-0.4 \lesssim \alpha_z \lesssim 1.2$) the system exhibits periodic states. For small anisotropies, this behavior can be explained by

the fact that nonlinear terms are small and the constant field plays the major role in the dynamics. For negative values of α_x almost above the curve with equation, $\alpha_z = 0.04165\alpha_x^2 + 0.45833\alpha_x + 4.25$, the system behaves in a regular fashion. Note that inside the main chaotic areas there are still windows without chaos. On the other hand, the right panel of Figure 4 shows the diagram for a complete anisotropic particle ($\alpha_j \neq 0$). We can observe a similar pattern which is slightly rotated and elongated with respect to the previous frame. Here, the approximate line over which the system has regular states is given by $\alpha_z = 0.17\alpha_x^2 + 1.32\alpha_x + 3.5$, such that $\alpha_x < 0$.

The leftmost panel in Figure 5 displays a phase diagram as a function of the anisotropy coefficients α_x and α_y at $\alpha_z = 1.0$. This diagram shows symmetric behaviors under reflection about the diagonal line $\alpha_y = \alpha_x$. We call this diagonal $\alpha_{y(x)}$ and indicate it by a dashed line in the figure. For negative values of both constants one can observe that the states are periodic approximately inside the region, $\alpha_x^2 + \alpha_y^2 = 3.7^2$. The same happens for the region above the curve $\alpha_y = 0.0625\alpha_x^2 + 0.525\alpha_x + 3.3$ when $\alpha_x \lesssim 0.5$ and for the region below the curve $\alpha_y = -1.64\alpha_x^2 + 13.97\alpha_x - 28.46$ when $\alpha_x \gtrsim 2.6$. In the remaining areas the system is mainly chaotic but contains complex topological islands of regular behaviors. To explore in more detail the dynamical behaviors occurring in the diagonal line, $\alpha_{y(x)}$, the right panel of Figure 5 presents a comparison of the LLE and bifurcation diagrams of the angular variables (ϕ, θ) . By increasing the parameter, we observe that the system starts in a periodic state and makes an abrupt transition to a chaotic behavior. After that, an alternation of regular and chaotic behaviors is found upon further increase of $\alpha_{y(x)}$. In addition, with the comparison of the LLE and the bifurcation diagrams one can determine precisely the segments where the regular phases correspond to periodic or quasi-periodic states. For instance, quasi-periodic oscillations can be identified in range $(0.032, 1.77)$.

In order to illustrate different nonchaotic regimes appearing along the $\alpha_{y(x)}$ diagonal, in Figure 6 we show a 2D Poincaré section of (m_z, m_y) at time-intervals multiple of $2\pi/\Omega$, the time series of m_z , and its corresponding power spectrum $|S(\varpi)|$ for five representative values of $\alpha_{y(x)}$, namely $-3.5, -0.3, 0.95, 3.27$ and 4.95 . From this figure, one sees that for -3.5 and -0.3 the system presents periodic states, while the other three parameters exhibits more complex quasiperiodic behaviors. In fact for $\alpha_{y(x)} = 0.95$ the Poincaré section shows a semi-torus.

4. Final remarks. The dynamics of the magnetization of an anisotropic particle in the simultaneous presence of a constant and a periodic time-dependent external magnetic field has been studied in the framework of the Landau-Lifshitz-Gilbert equation.

In previous works, we investigated the control parameter space for particles under conditions of uniaxial anisotropy [15] and also when subjected to a quasiperiodic magnetic field[38]. In contrast, here we considered the more general situation of particles under bi-axial anisotropy. We determined the regions in control parameter space where positive Lyapunov exponents (chaos) exist and the theoretical boundaries for the thresholds of the chaotic regime. We performed extensive numerical calculations of Lyapunov exponents while varying simultaneously two selected control parameters. This resulted in detailed stability charts of the chaotic and regular phases as a function of these parameters.

In this more general situation, we now find anisotropy to play an important role in creating an additional number of novel possible dynamical behaviors for the particle.

For bi-axial particles, when the anisotropy coefficients have the same values, the 2D LLE-diagram exhibits a circular shape symmetry as a function of driving field amplitudes. In contrast, when the coefficients have different signs this circular symmetry is broken, but the LLE-diagram still displays a composed inversion mirror symmetry. We found driven anisotropic particles to present multiple transitions between regular and chaotic states.

An interesting type of localized islands of regular patterns was discovered inside the chaotic regions. Such structures display the same peculiar shrimp-shaped structure familiar from many other (non-magnetic) systems [27, 40, 21]. To our knowledge this is the first time that such structures are reported in the magnetic context. These structures are known to be linked to the universal class of dynamics observed in homoclinic Shilnikov chaos [53, 5], although it is also known that spirals of shrimps also appear in situations unrelated to Shilnikov chaos [23, 26]. The global organization of complex structures is still poorly understood, and magnetic particles offer an alternative system for further investigations.

In addition to a detailed classification of the chaotic regions, the phase diagrams reported here also display extended domains where regular behavior is predominant. Some time ago, the control space of a damped-driven Duffing oscillator was shown to display certain recurring complex structures [14] which resemble somewhat the ones seen here in Figures 2 and 3. It would be interesting to investigate if such resemblance indeed exists and what is the extension of these similarities, if any. Furthermore, it should be interesting to compute isospike diagrams [24, 25, 47, 31], i.e. phase diagrams displaying the number of spikes contained in one period of every periodic oscillation. As described in a recent review paper [29], such diagrams provide detailed information about the complexification of periodic patterns when parameters are tuned continuously.

Acknowledgments. LMP and HM acknowledge partial financial support from the Spanish Ministry of Science and Technology under Contract No. FIS2011-24642. JB acknowledges partial financial support from Spanish Ministry of Science and Technology under Contract No. FIS2011-28820-C02-02. JACG was supported by CNPq, Brazil, by the Deutsche Forschungsgemeinschaft through the Cluster of Excellence *Engineering of Advanced Materials*, and by the Max-Planck Institute for the Physics of Complex Systems, Dresden, in the framework of the Advanced Study Group on Optical Rare Events. AC and DL acknowledge partial financial support from Basal Program Center for Development of Nanoscience and Nanotechnology (CEDENNA) and Millennium Scientific Initiative, P10 – 022 – F. OJS acknowledges partial financial support from CONICYT-FONDECYT Postdoctoral program fellowship under grant 3130678. DL acknowledges the partial financial support from EPSRC under grant EP/L002922/1, FONDECYT 1120764 and UTA-project 8750-12.

REFERENCES

- [1] F. M. de Aguiar, A. Azevedo and S. M. Rezende, Characterization of strange attractors in spin-wave chaos, *Phys. Rev. B*, **39** (1989), 9448–9452.
- [2] H. A. Albuquerque and P. C. Rech, **Spiral periodic structure inside chaotic region in parameter-space of a Chua circuit**, *Int. J. Circuit Theory. App.*, **40** (2012), 189–194.
- [3] L. F. Alvarez, O. Pla and O. Chubykalo, **Quasiperiodicity, bistability, and chaos in the Landau-Lifshitz equation**, *Phys. Rev. B*, **61** (2000), 11613–11617.

- [4] I. V. Barashenkov, M. M. Bogdan and V. I. Korobov, **Stability diagram for the phase-locked soliton of the parametrically driven, damped nonlinear Schrödinger equation**, *Europhys. Lett.*, **15** (1991), 113–118.
- [5] R. Barrio, A. Shilnikov and L. P. Shilnikov, **Kneadings, symbolic dynamics and painting Lorenz chaos**, *Int. J. Bifur. Chaos*, **22** (2012), 1230016, 24pp.
- [6] R. Barrio, F. Blesa and S. Serrano, **Topological changes in periodicity hubs of dissipative systems**, *Phys. Rev. Lett.*, **108** (2012), 214102.
- [7] X. Batlle and A. Labarta, **Finite-size effects in fine particles: Magnetic and transport properties**, *J. Phys. D*, **35** (2002), R15–R42.
- [8] J. Becker, F. Rodelsperger, Th. Weyrauch, H. Benner, W. Just and A. Cenys, **Intermittency in spin-wave instabilities**, *Phys. Rev. E*, **59** (1999), 1622–1632.
- [9] M. Beleggia, S. Tandon, Y. Zhu and M. De Graef, **On the magnetostatic interactions between nanoparticles of arbitrary shape**, *J. Magn. Magn. Mater.*, **278** (2004), 270–284.
- [10] M. Beleggia and M. De Graef, **General magnetostatic shape–shape interactions**, *J. Magn. Magn. Mater.*, **285** (2005), L1–L10.
- [11] C. Bonatto, J. Garreau and J. A. C. Gallas, **Self-similarities in the frequency-amplitude space of a loss-modulated CO₂ laser**, *Phys. Rev. Lett.*, **95** (2005), 143905.
- [12] C. Bonatto and J. A. C. Gallas, **Periodicity hub and nested spirals in the phase diagram of a simple resistive circuit**, *Phys. Rev. Lett.*, **101** (2008), 054101.
- [13] C. Bonatto and J. A. C. Gallas, **Accumulation boundaries: Codimension-two accumulation of accumulations in phase diagrams of semiconductor lasers, electric circuits, atmospheric and chemical oscillators**, *Phil. Trans. R. Soc. A*, **366** (2008), 505–517.
- [14] C. Bonatto, J. A. C. Gallas and Y. Ueda, **Chaotic phase similarities and recurrences in a damped-driven Duffing oscillator**, *Phys. Rev. E*, **77** (2008), 026217.
- [15] J. Bragard, H. Pleiner, O. J. Suarez, P. Vargas, J. A. C. Gallas and D. Laroze, **Chaotic dynamics of a magnetic nanoparticle**, *Phys. Rev. E*, **84** (2011), 037202.
- [16] J. Cai, Y. Kato, A. Ogawa, Y. Harada, M. Chiba and T. Hirata, **Chaotic dynamics during slow relaxation process in magnon systems**, *J. Phys. Soc. Jap.*, **71** (2002), 3087–3091.
- [17] M. G. Clerc, S. Coulibaly and D. Laroze, **Interaction law of 2D localized precession states**, *Europhys. Lett.*, **90** (2010), 38005.
- [18] M. G. Clerc, S. Coulibaly and D. Laroze, **Localized waves in a parametrically driven magnetic nanowire**, *Europhys. Lett.*, **97** (2012), 30006.
- [19] B. D. Cullity and C. D. Graham, ***Introduction to Magnetic Materials***, 2nd edition, J. Wiley IEEE Press, New Jersey, 2009.
- [20] W. L. Ditto, M. L. Spano, H. T. Savage, S. N. Rauseo, J. Heagy and E. Ott, **Experimental observation of a strange nonchaotic attractor**, *Phys. Rev. Lett.*, **65** (1990), 533–536.
- [21] W. Façanha, B. Oldeman and L. Glass, **Bifurcation structures in two-dimensional maps: The endoskeletons of shrimps**, *Phys. Lett. A*, **377** (2013), 1264–1268.
- [22] R. E. Francke, T. Pöschel and J. A. C. Gallas, **Zig-zag networks of self-excited periodic oscillations in a tunnel diode and a fiber-ring laser**, *Phys. Rev. E*, **87** (2013), 042907.
- [23] J. G. Freire and J. A. C. Gallas, **Non-Shilnikov cascades of spikes and hubs in a semiconductor laser with optoelectronic feedback**, *Phys. Rev. E*, **82** (2010), 037202.
- [24] J. G. Freire and J. A. C. Gallas, **Stern-Brocot trees in the periodicity of mixed-mode oscillations**, *Phys. Chem. Chem. Phys.*, **13** (2011), 12191–12198.
- [25] J. G. Freire and J. A. C. Gallas, **Stern-Brocot trees in cascades of mixed-mode oscillations and canards in the extended Bonhoeffer-van der Pol and the FitzHugh-Nagumo models of excitable systems**, *Phys. Lett. A*, **375** (2011), 1097–1103.
- [26] J. G. Freire, C. Cabeza, A. Martí, T. Pöschel and J. A. C. Gallas, **Antiperiodic oscillations**, *Nature Sci. Rep.*, **3** (2013), 01958.
- [27] J. A. C. Gallas, **Structure of the parameter space of the Hénon map**, *Phys. Rev. Lett.*, **70** (1993), 2714–2717.
- [28] J. A. C. Gallas, **The structure of infinite periodic and chaotic hub cascades in phase diagrams of simple autonomous flows**, *Int. J. Bifur. Chaos*, **20** (2010), 197–211; and references therein.
- [29] M. R. Gallas, M. R. Gallas and J. A. C. Gallas, **Distribution of chaos and periodic spikes in a three-cell population model of cancer**, *Eur. Phys. J. Special Topics*, **223** (2014), 2131–2144.
- [30] G. Gibson and C. Jeffries, **Observation of period doubling and chaos in spin-wave instabilities in yttrium iron garnet**, *Phys. Rev. A*, **29** (1984), 811–818.
- [31] A. Hoff, D. T. da Silva, C. Manchein and H. A. Albuquerque, **Bifurcation structures and transient chaos in a four-dimensional Chua model**, *Phys. Lett. A*, **378** (2014), 171–177.

- [32] M. Lakshmanan, [The fascinating world of the Landau-Lifshitz-Gilbert equation: An overview](#), *Philos. Trans. R. Soc. Lond. Ser. A Math. Phys. Eng. Sci.*, **369** (2011), 1280–1300.
- [33] P. Landeros, J. Escrig, D. Altbir, D. Laroze, J. d’Albuquerque e Castro and P. Vargas, [Scaling relations for magnetic nanoparticles](#), *Phys. Rev. B*, **65** (2005), 094435.
- [34] D. Laroze and P. Vargas, [Dynamical behavior of two interacting magnetic nanoparticles](#), *Phys. B*, **372** (2006), 332–336.
- [35] D. Laroze and L. M. Perez, [Classical spin dynamics of four interacting magnetic particles on a ring](#), *Phys. B*, **403** (2008), 473–477.
- [36] D. Laroze, P. Vargas, C. Cortes and G. Gutierrez, [Dynamics of two interacting dipoles](#), *J. Magn. Magn. Mater.*, **320** (2008), 1440–1448.
- [37] D. Laroze, O. J. Suarez, J. Bragard and H. Pleiner, [Characterization of the chaotic magnetic particle dynamics](#), *IEEE Trans. On Magnetics*, **47** (2011), 3032–3035.
- [38] D. Laroze, D. Becerra-Alonso, J. A. C. Gallas and H. Pleiner, [Magnetization dynamics under a quasiperiodic magnetic field](#), *IEEE Trans. On Magnetics*, **48** (2012), 3567–3570.
- [39] D. Laroze, P. G. Siddheshwar and H. Pleiner, [Chaotic convection in a ferrofluid](#), *Commun. Nonlinear Sci. Numer. Simulat.*, **18** (2013), 2436–2447.
- [40] E. N. Lorenz, [Compound windows of the Hénon map](#), *Physica D*, **237** (2008), 1689–1704.
- [41] D. Mayorgoz, G. Bertotti and C. Serpico, *Nonlinear Magnetization Dynamics in Nanosystems*, Elsevier, North Holland, 2009; and references therein.
- [42] R. C. O’Handley, *Modern Magnetic Materials: Principles and Applications*, Wiley Inter-science, New York, 1999.
- [43] D. F. M. Oliveira, M. Robnik and E. D. Leonel, [Shrimp-shape domains in a dissipative kicked rotator](#), *Chaos*, **21** (2011), 043122, 6pp.
- [44] L. M. Pérez, O. J. Suarez, D. Laroze and H. L. Mancini, [Classical spin dynamics of anisotropic Heisenberg dimers](#), *Cent. Eur. J. Phys.*, **11** (2013), 1629–1637.
- [45] A. Sack, J. G. Freire, E. Lindberg, T. Pöschel and J. A. C. Gallas, [Discontinuous spirals of stable periodic oscillations](#), *Nature Sci. Rep.*, **3** (2013), 03350.
- [46] R. K. Smith, M. Grabowski and R. E. Camley, [Period doubling toward chaos in a driven magnetic macrospin](#), *J. Magn. Magn. Mater.*, **322** (2010), 2127–2134.
- [47] S. L. T. Souza, A. A. Lima, I. R. Caldas, R. O. Medrano-T and Z. O. Guimães-Filho, [Self-similarities of periodic structures for a discrete model of a two-gene system](#), *Phys. Lett. A*, **376** (2012), 1290–1294.
- [48] S. Tandon, M. Beleggia, Y. Zhu and M. De Graef, [On the computation of the demagnetization tensor for uniformly magnetized particles of arbitrary shape. Part I: Analytical approach](#), *J. Magn. Magn. Mater.*, **271** (2004), 9–26.
- [49] S. Tandon, M. Beleggia, Y. Zhu and M. De Graef, [On the computation of the demagnetization tensor for uniformly magnetized particles of arbitrary shape. Part II: Numerical approach](#), *J. Magn. Magn. Mater.*, **271** (2004), 27–38.
- [50] D. Urzagasti, D. Laroze, M. G. Clerc and H. Pleiner, [Breather soliton solutions in a parametrically driven magnetic wire](#), *Europhys. Lett.*, **104** (2013), 40001.
- [51] D. Urzagasti, A. Aramayo and D. Laroze, [Soliton-antisoliton interaction in a parametrically driven easy-plane magnetic wire](#), *Phys. Lett. A*, **378** (2014), 2614–2618.
- [52] D. V. Vagin and P. Polyakov, [Control of chaotic and deterministic magnetization dynamics regimes by means of sample shape varying](#), *J. App. Phys.*, **105** (2009), 033914.
- [53] R. Vitolo, P. Glendinning and J. A. C. Gallas, [Global structure of periodicity hubs in Lyapunov phase diagrams of dissipative flows](#), *Phys. Rev. E*, **84** (2011), 016216.
- [54] P. E. Wigen (Ed.), *Nonlinear Phenomena and Chaos in Magnetic Materials*, World Scientific, Singapore, 1994.
- [55] A. Wolf, J. B. Swift, H. L. Swinney and J. A. Vastano, [Determining Lyapunov exponents from a time series](#), *Physica D*, **16** (1985), 285–317.

Received July 2014; revised December 2014.

E-mail address: lperez.17@alumni.unav.es

E-mail address: jbragard@unav.es

E-mail address: hmancini@unav.es

E-mail address: jgallas@fisica.ufpb.br

E-mail address: ana.cabanas.plana@gmail.com

E-mail address: ojsuarez1@yahoo.com

E-mail address: dlarozen@uta.cl